Near-infrared branding efficiently correlates light and electron microscopy

Derron Bishop[1], Ivana Nikić[2], Mary Brinkoetter[1], Sharmon Knecht[1], Stephanie Potz[2,3], Martin Kerschensteiner[2,5] & Thomas Misgeld[3–5]

The correlation of light and electron microscopy of complex tissues remains a major challenge. Here we report near-infrared branding (NIRB), which facilitates such correlation by using a pulsed, near-infrared laser to create defined fiducial marks in three dimensions in fixed tissue. As these marks are fluorescent and can be photo-oxidized to generate electron contrast, they can guide re-identification of previously imaged structures as small as dendritic spines by electron microscopy.

Many areas of biology have benefited from advances in light microscopy, which can be used to monitor cellular behavior in tissue[1]. One limitation, however, is that subcellular machinery is beyond the resolution of conventional light microscopy. Currently, electron microscopy remains the most commonly used technique to visualize subcellular structures in preserved tissue[2], but for mechanistic interpretation, electron micrographs often need to be correlated to their light microscopic counterparts. Such correlations still face substantial technical obstacles, especially in intact tissues, in which a cell that had been previously imaged by light microscopy has to be distinguished from many other similar cells. Previous approaches to overcome this challenge[3–8] often used photo-oxidation of fluorophores, enzymatic reactions (for example, mediated by horseradish peroxidase (HRP)) or ultrasmall gold particles to create electron-dense markers selectively in the cell of interest. For this purpose, small-molecule fluorescent dyes and HRP can be used directly as tracers that are either actively taken up by cells, loaded into single cells via microcapillaries, or conjugated to antibodies or avidin to target them to cell populations of interest. HRP can also be transgenically expressed[9]. Although very powerful, these approaches still have major drawbacks. (i) In uniformly labeled cell populations, high epitope density can make finding relevant structures cumbersome. (ii) The deposition of an electron-dense precipitate in the structure of interest can obscure ultrastructural detail. (iii) The mild fixation and harsh permeabilization conditions required for antibody labeling can compromise ultrastructure. (iv) Delivery of tracers or neo-epitopes to living tissue requires surgical access, can take time and can cause toxic side effects. (v) Transgenic delivery of HRP requires genetic manipulations, which, at least in mammals, can be slow and resource-consuming. (vi) For correlating *in vivo* imaging and electron microscopy, special concerns arise, as the least toxic *in vivo* labels (for example, GFP) are generally poor photo-oxidizers and vice versa.

These drawbacks preclude the widespread use of correlated light and electron microscopy, especially in intact tissue. Still, in cases when these problems have been overcome, important insights into subcellular biology have been made[2–4,10], motivating a quest for a more generally applicable solution. One such approach is the use of fiducial marks that have both optical and electron contrast. These can either be endogenous (blood vessels or characteristic sparse cellular structures) or exogenous (fluorescent beads or etched grids in cell culture). But endogenous fiducial marks are not present in all tissues with high enough density to sufficiently reduce the search volume, and exogenous marks are difficult to introduce into intact tissue. Indeed, in most cases, exogenous fiducial marks are added after ultrathin sectioning (for example, by 'sprinkling' beads on sections[11]). Thus, it would be desirable to develop an approach that allows targeted placement of fiducial marks into any intact tissue.

Here we report near-infrared branding (NIRB), which can be used to accomplish this and overcome many drawbacks of previous approaches. NIRB uses a femtosecond pulsed titanium-sapphire laser to create fiducial 'branding' marks in defined three-dimensional positions in tissue fixed for electron microscopy (**Fig. 1a–c** and **Supplementary Video 1**). We tuned the laser wavelength to 910 nm and used line scans (pixel dwell time, 2–20 µs) or point scans to generate user-defined patterns of NIRB marks. The size of these marks can be determined by the dose of pulsed light (**Fig. 1d** and **Supplementary Video 2**). NIRB marks can thus be placed with micrometer precision in the immediate vicinity of a structure of interest. Notably, these marks are autofluorescent and by virtue of their characteristic spectral signature (**Fig. 1e**) can be re-identified by light microscopy. This autofluorescence also permits selective photo-oxidation of NIRB marks. Photo-oxidation generates a marker for electron microscopic identification in the immediate vicinity of the structure of interest, but not in the structure itself, as GFP is not photo-oxidized at the same time (**Fig. 1f** and **Supplementary Fig. 1**). After processing and embedding the

[1]Department of Physiology, Indiana University School of Medicine–Muncie, Muncie, Indiana, USA. [2]Research Unit Therapy Development, Institute of Clinical Neuroimmunology, Ludwig Maximilians University, Munich, Germany. [3]Biomolecular Sensors and Center for Integrated Protein Sciences (Munich) at the Institute of Neuroscience, Technical University Munich, Munich, Germany. [4]Technical University Munich Institute for Advanced Study, Munich, Germany. [5]These authors contributed equally to this work. Correspondence should be addressed to T.M. (thomas.misgeld@lrz.tu-muenchen.de) or M.K. (martin.kerschensteiner@med.uni-muenchen.de).

RECEIVED 19 JANUARY; ACCEPTED 22 APRIL; PUBLISHED ONLINE 5 JUNE 2011; DOI:10.1038/NMETH.1622

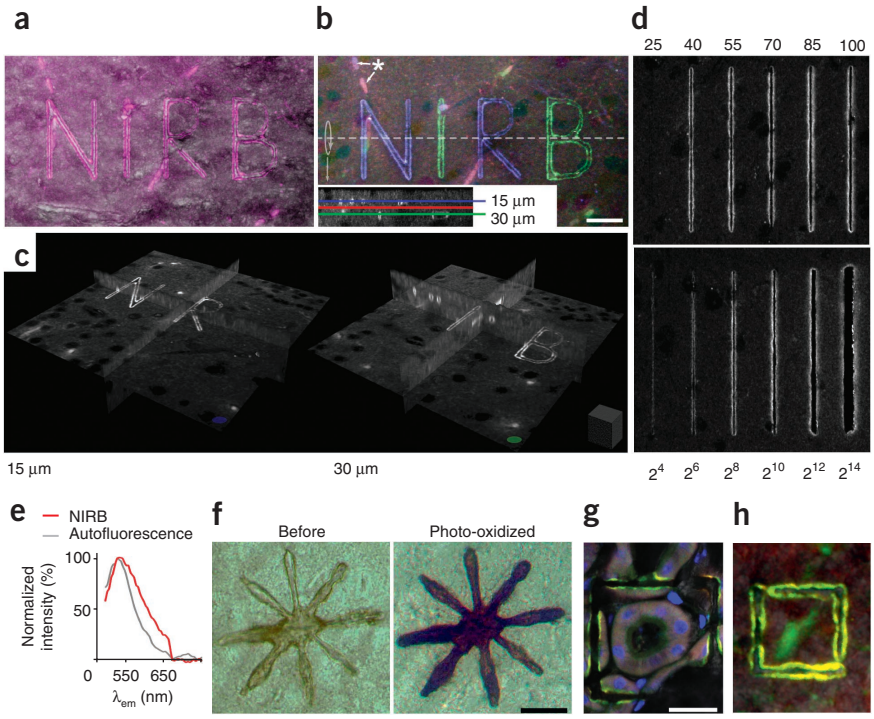

Figure 1 | Defined induction of fiducial marks by NIRB. (**a**–**c**) Two-photon images of NIRB marks in glutaraldehyde-fixed vibratome sections of mouse cerebral cortex. Maximum intensity projection with overlay of transillumination image (grayscale) and NIRB fluorescence (magenta) (**a**). Pseudocolored projection of three planes (inset, *x*–*z* projection) (**b**); the letters N and R were burned at a depth of 15 µm, whereas I and B were burned at a depth of 30 µm; an intermediate depth is shown in red. Erythrocytes show autofluorescence (asterisk). Three-dimensional rendering (**c**) showing the position of the 15 µm (left) and 30 µm (right) planes relative to the orthogonal projections. (**d**) Images of NIRB marks made with line scans of increasing percentages of laser power (top) and increasing numbers of laser swipes (bottom); scan line length, 106 µm. (**e**) Fluorescence emission spectrum (λ_{em}) of NIRB marks compared to tissue autofluorescence after excitation with a 488-nm laser (normalized intensity as percentage of maximum). (**f**) Transmitted light images of an NIRB mark before (left) and after (right) photo-oxidation using diaminobenzidine. (**g**,**h**) NIRB marks of a kidney tubule (**g**; nuclei, blue) or a macrophage in a lymph node (**h**; GFP labeling in a *Cx3cr1*$^{GFP/+}$ mouse, green). Scale bars, 25 µm (**a**,**b**), 50 µm (**f**) and 25 µm (**g**,**h**). Scale cube in **c** has a border length of 25 µm.

tissue, NIRB marks were thus readily detectable in 0.5-µm-thick plastic sections examined by light microscopy (**Supplementary Fig. 1**). The target area, containing a structure of interest, could then be identified in subsequently prepared serial ultrathin sections, as NIRB marks were recognizable as tissue defects surrounded by electron-dense precipitates, and registered with the light microscopy image. When using a high numerical aperture (NA) objective (for example, 60×, 1.42 NA oil), we estimate that NIRB marks can be placed as close as 3–4 µm with little risk of destroying a structure between the marks (Online Methods and **Supplementary Fig. 2**). As NIRB marks have a *z*-dimension extension of about 4 µm, the minimal marked volume can be smaller than 70 µm^3. Even for tissue as complex as the brain, volumes of this size can be segmented and proofread completely with current segmentation algorithms in hours[12]. NIRB provides additional information in the form of the confocally determined relative *x*-*y*-*z* position of a structure of interest from the induced marks, increasing localization precision. Finally, NIRB is widely applicable, as branding marks can be made in a variety of tissues (**Fig. 1g**,**h**) derived from different species (for example, zebrafish; data not shown).

To test NIRB, we targeted individual spines on apical dendrites of fluorescently labeled cortical neurons in transgenic *Thy1-GFP*,

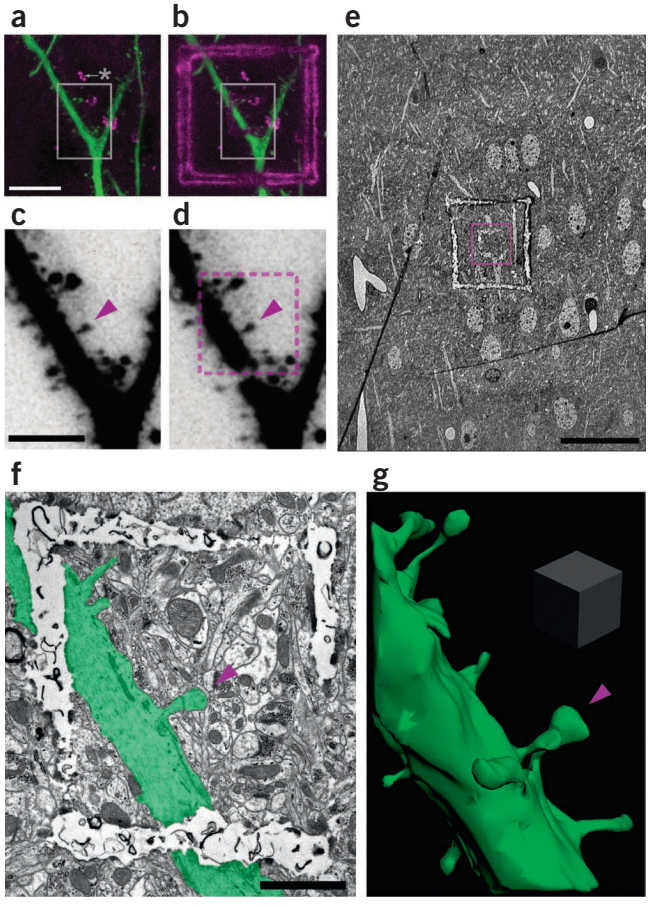

Figure 2 | NIRB allows re-identification and electron microscopic reconstruction of dendritic spines. (**a**,**b**) Confocal projections of apical dendrites in a cortical vibratome section of a *Thy1-GFP*^{S} mouse, before (**a**) and after (**b**) NIRB marking. Asterisk indicates autofluorescent lipofuscin granules. (**c**,**d**) Magnified and contrast-inverted views of the boxed regions in **a** and **b** (arrowheads indicate the targeted spine) before (**c**) and after (**d**) NIRB marking. The inner NIRB box with a border length of 6.5 µm is shown by the dashed magenta line. (**e**) Low-power electron micrograph of the target region after switching from thick sectioning to ultrathin sectioning. The outer NIRB box is easily detected. The inner box is surrounded by a magenta outline. (**f**) Ultrathin section through the targeted spine (arrowhead) and its dendrite (pseudocolored green). The inner NIRB box is evident. (**g**) Three-dimensional rendering of spine (arrowhead) based on tracings in serial electron micrographs. Scale bars, 10 µm (**a**,**b**), 5 µm (**c**,**d**), 25 µm (**e**), 2 µm (**f**) and scale cube in **g** has a border length of 1 µm.

line S (*Thy1-GFP*^{S}) mice. For reidentification by serial-sectioning transmission electron microscopy, we first documented the dendrite (and spines) in the fixed vibratome sections by collecting both low- and high-resolution image stacks on a confocal microscope using 20×, 0.85 NA or 60×, 1.42 NA oil-immersion objectives. We then transferred the slide with the fixed vibratome section to the multiphoton setup and used NIRB to burn a large box (about 25 µm × 25 µm; **Fig. 2a–d**) about 1 µm superficial to the spine and a small box (6.5 µm × 6.5 µm) at the level of a spine. Then we photo-oxidized the NIRB marks and trimmed the brain slice with a razor blade to ~2 mm × 2 mm in the *x-y* dimension. There was no risk of trimming away the area of interest because the larger photo-oxidized box could be easily visualized using a dissecting microscope. We processed photo-oxidized vibratome sections for electron microscopy and could identify the large box on semi-thin sections examined by light microscopy (**Supplementary Fig. 1d**). Once we identified the large box, we trimmed the block further and began cutting serial ultrathin sections that we examined in the transmission electron microscope. We identified the small box (**Fig. 2e**), which allowed unequivocal re-identification and serial electron microscopic reconstruction of the spine of interest (**Fig. 2f**,**g** and **Supplementary Video 3**). For the example shown in **Figure 2**, the reconstruction revealed the presence of a second closely apposed spine, which was contained in the same diffraction-limited volume as the spine originally identified by confocal microscopy.

We also used NIRB to reconstruct individual GFP-labeled sensory axons after a spinal cord lesion (**Supplementary Fig. 3**). We first imaged axons before and after transection in the spinal cord of living mice with sparse transgenic axon labeling[13] and identified a structure of interest (an axonal end bulb) *in vivo* (**Supplementary Fig. 3**). After fixation for electron microscopy, we imaged the axon end bulb with confocal microscopy and then used NIRB to mark it, permitting us to re-identify it in plastic-embedded sections and reconstruct it by serial-sectioning transmission electron microscopy (**Supplementary Fig. 3**). The efficiency of this procedure in our hands exceeded 80% (we identified the structure of interest in 9 of 11 cases, with 7 fully reconstructed).

NIRB can be used in a wide variety of tissues and applications. It will be a versatile tool to obtain ultrastructural detail of optically imaged structures, impart a dynamic context to electron microscopy and focus electron-microscopic reconstruction efforts to small, relevant areas of large tissue blocks. As both optical imaging and electron microscopy are undergoing a parallel renaissance, with optical nanoscopy probing the subcellular domain[11] and large-scale automated electron microscopic reconstruction methods approaching the mesoscale[14,15], spanning the resolution gap between such techniques is becoming an increasingly important challenge, which NIRB can help to meet.

METHODS

Methods and any associated references are available in the online version of the paper at http://www.nature.com/naturemethods/.

Note: Supplementary information is available on the Nature Methods website.

ACKNOWLEDGMENTS

We thank L. Godinho for critical reading of the manuscript. This work was supported by grants to M.K. and T.M. from the Dana Foundation and the Hertie Foundation and a grant to T.M. and D.B. from the Christopher and Dana Reeve Foundation. D.B. is supported by the US National Institutes of Health. Work in M.K.'s laboratory is financed through grants from the Deutsche Forschungsgemeinschaft (Emmy-Noether Program, SFB 571 and SFB 870), the German Federal Ministry of Research and Education (Competence Network Multiple Sclerosis) and the 'Verein Therapieforschung für MS-Kranke e.V.' T.M. is supported by the Institute of Advanced Study (Technische Universität München), the Deutsche Forschungsgemeinschaft (SFB 596), the Bundesministerium für Bildung und Forschung (ERA-Net 'two-photon imaging'), the Alexander von Humboldt Foundation and the Center for Integrated Protein Science (Munich).

AUTHOR CONTRIBUTIONS

D.B., M.K. and T.M. conceived the experiments. I.N., S.P., M.K. and T.M. performed *in vivo* imaging and near-infrared branding experiments. M.B., S.K. and D.B. performed correlated serial electron microscopy. M.K., T.M. and D.B. wrote the paper.

COMPETING FINANCIAL INTERESTS

The authors declare no competing financial interests.

Published online at http://www.nature.com/naturemethods/.
Reprints and permissions information is available online at http://www.nature.com/reprints/index.html.

1. Lichtman, J.W. & Fraser, S.E. *Nat. Neurosci.* **4** (Suppl), 1215–1220 (2001).
2. Bourne, J.N. & Harris, K.M. *Annu. Rev. Neurosci.* **31**, 47–67 (2008).
3. Rhodin, J.A. & Fujita, H.J. *Submicrosc. Cytol. Pathol.* **21**, 1–34 (1989).
4. Polishchuk, R.S. *et al. J. Cell Biol.* **148**, 45–58 (2000).
5. Mironov, A.A. & Beznoussenko, G.V. *J. Microsc.* **235**, 308–321 (2009).
6. Grabenbauer, M. *et al. Nat. Methods* **2**, 857–862 (2005).
7. Sosinsky, G.E., Giepmans, B.N., Deerinck, T.J., Gaietta, G.M. & Ellisman, M.H. *Methods Cell Biol.* **79**, 575–591 (2007).
8. Knott, G.W., Holtmaat, A., Trachtenberg, J.T., Svoboda, K. & Welker, E. *Nat. Protoc.* **4**, 1145–1156 (2009).
9. Li, J., Erisir, A. & Cline, H. *Neuron* **69**, 273–286 (2011).
10. Darcy, K.J., Staras, K., Collinson, L.M. & Goda, Y. *Nat. Neurosci.* **9**, 315–321 (2006).
11. Watanabe, S. *et al. Nat. Methods* **8**, 80–84 (2011).
12. Mishchenko, Y. *et al. Neuron* **67**, 1009–1020 (2010).
13. Kerschensteiner, M., Schwab, M.E., Lichtman, J.W. & Misgeld, T. *Nat. Med.* **11**, 572–577 (2005).
14. Denk, W. & Horstmann, W. *PLoS Biol.* **2**, e329 (2004).
15. Knott, G., Marchman, H., Wall, D. & Lich, B. *J. Neurosci.* **28**, 2959–2964 (2008).

ONLINE METHODS

Animals. We used the following transgenic and knock-in mice: *Thy1-GFP*^{S} mice were used to label a small subset of neurons and their processes with GFP[16] (mice were a gift of J. Sanes and J. Lichtman, Harvard University). *Cx3cr1*$^{GFP/+}$ mice (Jackson Laboratory strain designation: *Cx3cr1*^{tm1Litt}*/J)* were used to label macrophages[17] (mice were a gift from D. Littman, New York University). C57BL/6 (Elevage Janvier) wild-type mice were used as a source of unlabeled tissue. All animal work conformed to institutional guidelines and was approved by the Animal Study Committee of the Regierung von Oberbayern, Germany.

Transection and *in vivo* imaging of spinal axons. We imaged lesioned individual GFP-labeled axons in *Thy1-GFP*^{S} mice as previously described[13,18]. Briefly, mice were anesthetized by an intraperitoneal injection of ketamine-xylazine (87 mg kg^{-1} ketamine and 13 mg kg^{-1} xylazine). To access the spinal cord, a laminectomy was performed, and the dorsal surface of the spinal cord was exposed. During the imaging session, the spinal cord was superfused with prewarmed Ringer's solution or mouse artificial cerebrospinal fluid. Individual GFP-labeled axons were identified using a fluorescence dissecting microscope (Olympus SZX16) and cut under visual control using a hand-held 23 G needle. Axons were documented before and at multiple timepoints after transection using a wide-field setup based on an Olympus BX51 microscope equipped with 4×, 0.13 NA air, 10×, 0.3 NA and 20×, 0.5 NA dipping cone water-immersion objectives and a cooled Sensicam QE charge-coupled device (CCD) camera (pco/ Visitron) controlled by MetaMorph software (Universal Imaging). Image streams of 25 to 30 images were acquired for each field and timepoint.

Tissue fixation and processing. We perfused mice transcardially with 2.5% electron microscopy grade glutaraldehyde and 2.0% paraformaldehyde in 0.1 M PBS (pH 7.2) (Electron Microscopy Sciences). We then post-fixed the tissue for 2 h (lymph nodes and kidneys) to 24 h (spinal cords and brains). We obtained similar tissue quality independent of the fixation time, indicating that longer fixation times were not required. To determine the extent to which GFP fluorescence bleached with different post-fixation intervals, we perfused *Thy1-GFP*^{S} mice as described above. After dissection, we imaged the same spinal cord whole mounts by confocal microscopy after different time intervals of fixation (1, 3, 24 and 72 h). We then measured the average fluorescence intensity in and outside the same fluorescently labeled axons over time using the ImageJ-based open-source Fiji software package. Fluorescence signal over background decreased by about 30% over the first hour after perfusion (average fluorescence over background was 1,062 ± 141 a.u. (mean ± s.e.m.) immediately after perfusion versus 700 ± 78 a.u. at 1 h after fixation, n = 14–15 axons, 3 mice) but then changed much more slowly during the remainder of the examination period (average fluorescence was 493 ± 56 a.u. versus 387 ± 46 a.u. at 24 and 72 h after fixation, respectively).

After fixation, the tissue of interest (for example, a spinal cord containing a previously imaged axon) was cut into thick (100–150 µm) sections using a vibratome. These sections were temporarily mounted in PBS under a coverslip in imaging chambers built using Parafilm spacers on a glass slide.

Near-infrared branding. We made NIRB marks using either a custom-built multiphoton imaging setup based on an Olympus FV300 scanner[19] or the commercially available Olympus FV1000MPE, each equipped with a femtosecond-pulsed titanium-sapphire laser (Mai Tai, Newport/Spectra-Physics). Attenuation was accomplished with a polarizing beam splitter on the FV300 system and with acousto-optical modulators on the FV1000MPE microscope. The size of NIRB marks was regulated by modulating laser power and exposure time (**Fig. 1d**). The precise relationship between laser dose and mark size depended on the z-depth of a mark, as tissue attenuates the laser. Unless stated otherwise, we used unattenuated laser power for branding (~200 mW in the back-focal plane). To visualize NIRB marks, we collected two-photon or confocal image stacks (images spaced at 0.3–1 µm intervals) of the structure of interest before and after branding using emission filters for yellow-green fluorescent proteins (for example, 520–560 nm). NIRB marks were visualized using DsRed emission filters (for example, 575–630 nm). Additionally, a transmitted light image was collected using a fiberoptically coupled substage detector. We used 4×, 0.1 NA air, 60×, 1.42 NA oil-immersion and 20×, 0.5 NA, 25×, 1.05 NA, 60×, 0.9 NA dipping cone water-immersion objectives for documentation; the 60×, 1.42 NA oil-, 25×, 1.05 NA water- and 60×, 0.9 NA water-immersion objectives were used to set NIRB marks. For **Supplementary Video 2**, we used a secondary scanner on the FV1000MPE system that allows setting NIRB marks with a second near-infrared laser beam (tuned to 720 nm), interdigitated with imaging using the primary scanner. To measure emission spectra, the lambda scan function of the FV1000 confocal system was used for 488-nm excitation.

Correlated serial electron microscopic reconstruction. To obtain correlated electron micrographs, we documented the structure of interest in the fixed vibratome sections by collecting both low- and high-resolution image stacks on a confocal microscope (Olympus FV1000) using 20×, 0.85 NA or 60×, 1.42 NA oil-immersion objectives. We then transferred the slide to the multiphoton setup to mark the structure of interest using NIRB as described above.

To locate identified dendritic spines, we burned a ~25 µm × 25 µm box 1.0 µm superficial to the area of interest. We then burned a smaller box (~6.5 µm × 6.5 µm) at the same depth as the dendritic spine (**Fig. 2** and **Supplementary Fig. 1**). We used a similar strategy for locating individual axons in the spinal cord with the exception of adding a small circular spot (1–2 µm) in the spinal cord adjacent to the axon of interest (**Supplementary Fig. 3c**). In both cases, we documented the fluorescence generated by NIRB marks using confocal microscopy as described.

The imaging chambers were cut open to remove the vibratome sections. The sections were pinned in Sylgard-lined 35 mm Petri dishes (Sylgard silicone elastomer, Dow Corning Corporation). The preparation was bathed in 5.0 mg ml^{-1} diaminobenzidine in 0.1 M Tris buffer (pH 7.4). The NIRB marks were then photo-oxidized by exciting the sample at 520–560 nm for ~20 min with a 40×, 0.8 NA water-immersion objective. After photo-oxidation, the fluorescence was replaced with a brown diaminobenzidine precipitate (**Fig. 1f** and **Supplementary Fig. 1**). After trimming, the photo-oxidized vibratome sections were processed for electron microscopy by staining with 1.0% osmium tetroxide reduced

in 1.5% potassium ferrocyanide (1 h), washed in four changes of 0.1 M sodium cacodylate buffer and dehydrated in an ascending ethanol series. After dehydration, tissue blocks were submerged twice in 100% propylene oxide, infiltrated with Araldite 502/EMbed812 resin (Electron Microscopy Sciences), flat-embedded into the cap of inverted embedding capsules (BEEM) and polymerized at 60 °C for 48 h. Thick sections (0.5–1.0 µm) were cut from the embedded tissue block with a glass knife and examined with transmitted light until the photo-oxidized NIRB markings became visible in the light microscope (**Supplementary Fig. 1d**). The tissue block was then trimmed to contain the region of interest for ultrathin serial sectioning as previously described[20]. Serial sections (50–70 nm) were cut from the block and then examined for the NIRB markings (**Fig. 2e**).

Considerations to determine precision limits of NIRB. We used brain tissue to estimate the smallest volume of tissue that can be reproducibly enclosed by NIRB marks in three dimensions. Based on our experience, the limiting factor was the unevenness of the outer borders of the NIRB marks, which might be determined by local tissue variations and formation of gas bubbles (**Supplementary Video 2**). Other variables seem less important: for example, the precision with which lines can be placed with a laser-scanning microscope is high and the rim of tissue that is obscured by burn damage and photo-oxidation is small (<100 nm; **Fig. 2f**). In contrast, the thickness of typical NIRB lines showed substantial variability (1.2 ± 0.3 µm, mean ± s.d. from center of line to outer border for the small lines used to enclose spines; **Fig. 2b** and **Supplementary Fig. 2b**,**c**). This suggests that to reduce the risk of inadvertently burning a structure of interest (for example, of about 1–2 µm in size), the distance between the centers of two parallel NIRB marks should at least be separated by about 6–7 µm (2 × mean half width of marks plus 2 × 4 s.d. plus object size). Considering the distance from the center to the border of the NIRB line (about 1.2 µm, see above), the inner borders of the parallel lines were thus spaced apart by about 4 µm. Given the depth of such a line of roughly 4 µm (**Supplementary Fig. 2e**) the volume within such a box (~4 × 4 µm inner diameter) would then be ~64 μm^3 (**Supplementary Fig. 2f**). Two other factors should be fathomed into this consideration. First, tissue can distort during processing and in the electron beam; second, NIRB marks can form irregular shapes, when bubbles get trapped, for example, in vessels. But both limitations can be overcome: NIRB marks actually offer a direct reference for correcting distortions (for example, the box in **Fig. 2e** needed to be stretched by −6% in the vertical direction to match the light microscopic view in **Fig. 2b**). Furthermore, NIRB marks do not need to be placed in any specific pattern. As autofluorescence generally allows seeing vessels in the background of a confocal image (data not shown) NIRB marks can be placed away from such structures.

Image processing. Fiji (downloaded from pacific.mpi-cbg.de/wiki/index.php/fiji), a distribution package of ImageJ, and Photoshop (Adobe) were used for image processing and figure representation. Confocal and two-photon image stacks were presented as maximum intensity projections unless stated otherwise. For **Figure 1c**, the '3D-Viewer' of Fiji was used to generate orthoslice projections. Photoshop's 'despeckle' function was used to suppress detector noise. Gamma settings were adjusted nonlinearly to better represent faint details, except for when processing images that illustrate intensity distributions (**Fig. 1d**).

We measured emission spectra using Fiji. Mean gray values of NIRB marks were measured in a fitted region of interest. We subtracted surrounding background, normalized the measurements to peak values, and converted the resulting distributions into graphs using Excel (Microsoft).

For quantification of NIRB marks (**Supplementary Fig. 2**), we generated *x*–*y* and *z*–*y* confocal projections with Fiji, which we median-filtered to suppress detector noise, contrast-adjusted and converted to gray value depth of 8 bits. We used 'auto-thresholding' plug-ins (based on the 'Li' or 'Otsu' algorithms), followed by 'close', 'fill-in' and 'outline' functions to generate binary outlines, along which we measured the width of the NIRB marks every 0.6 µm. Outliers that were due to burning inside vessel structures were excluded from this estimate. For representation, we manually centered several NIRB marks and outlines and used an average intensity projection to generate a collapsed view.

Electron micrographs were captured at 75 kV with a Hitachi H600 transmission electron microscope, individually scanned with an Epson Perfection V700 photo scanner, montaged with Panvue Image Assembler (PanaVue) and imported into Reconstruct[21]. The sections were aligned, and surface contours of axons were manually traced in Reconstruct. Contours were tessellated into three-dimensional Boissonnant surface models and rendered using 3ds Max (Autodesk). For the low-power electron micrograph in **Figure 2e**, a high-pass filter was used to remove background staining gradients.

16. Feng, G. *et al. Neuron* **28**, 41–51 (2000).
17. Jung, S. *et al. Mol. Cell. Biol.* **20**, 4106–4114 (2000).
18. Misgeld, T., Nikic, I. & Kerschensteiner, M. *Nat. Protoc.* **2**, 263–268 (2007).
19. Majewska, A., Yiu, G. & Yuste, R. *Pflugers Arch.* **441**, 398–408 (2000).
20. Bishop, D., Misgeld, T., Walsh, M.K., Gan, W.B. & Lichtman, J.W. *Neuron* **44**, 651–661 (2004).
21. Fiala, J.C. *J. Microsc.* **218**, 52–61 (2005).

doi:10.1038/nmeth.1622